The Astrophysical Journal, 719:1807–1812, 2010 August 20 doi:10.1088/0004-637X/719/2/1807

THE MASS AND RADIUS OF THE NEUTRON STAR IN 4U 1820−30

Tolga Güver, Patricia Wroblewski, Larry Camarota, and Feryal Özel
University of Arizona, Department of Astronomy, 933 N. Cherry Ave., Tucson, AZ 85721, USA
Received 2009 November 30; accepted 2010 July 1; published 2010 August 3

ABSTRACT

We report on the measurement of the mass and radius of the neutron star in the low-mass X-ray binary 4U 1820−30. The analysis of the spectroscopic data on multiple thermonuclear bursts yields well-constrained values for the apparent emitting area and the Eddington flux, both of which depend in a distinct way on the mass and radius of the neutron star. The distance to the source is that of the globular cluster NGC 6624, where the source resides. Combining these measurements, we uniquely determine the probability density over the stellar mass and radius. We find the mass to be $M = 1.58 \pm 0.06\,M_{\odot}$ and the radius to be $R = 9.1 \pm 0.4$ km.

Key words: stars: neutron – stars: individual (4U 1820−30) – X-rays: binaries

Online-only material: color figures

1. INTRODUCTION

One of the ways to measure the radii and masses of neutron stars is through a combination of spectroscopic phenomena observed from their surfaces. In particular, time-resolved spectra of thermonuclear X-ray bursts provide a measure of the apparent effective area of the neutron star over a wide range of temperatures. Furthermore, very luminous X-ray bursts (called photospheric radius expansion, or PRE, bursts) cross the local Eddington flux at the neutron star surface and allow us to obtain a measure of the neutron star mass that is corrected for general relativistic effects. In the absence of a third spectroscopic quantity, such as a redshifted absorption line, converting the observed quantities to masses and radii requires a knowledge of the distance to the X-ray source. Özel et al. (2009) and Güver et al. (2010) recently measured the masses and radii of the neutron stars in two low-mass X-ray binaries using this approach.

Low-mass X-ray binaries located in globular clusters allow for a convenient application of this method because their distances can be determined by utilizing the optical and near infrared observations of the globular clusters (see, e.g., Harris 1996; Valenti et al. 2007). Here, we report on the mass and radius of a third neutron star, the compact object in the binary 4U 1820−30, that resides in the globular cluster NGC 6624. 4U 1820−30 is an ultra-compact binary with an orbital period of 11.4 minutes (Stella et al. 1987). The short period of the system implies a low-mass, Roche lobe-filling, degenerate dwarf companion with a mass of about $\sim 0.07\,M_{\odot}$ (see, e.g., Stella et al. 1987; Verbunt 1987, Arons & King 1993; Anderson et al. 1997).

Thermonuclear X-ray bursts from the source were first discovered by Grindlay et al. (1976). Five type-I X-ray bursts, all showing evidence of photospheric radius expansion, have been reported from an analysis of *Rossi X-ray Timing Explorer* (*RXTE*) data (Galloway et al. 2008; see also Zdziarski et al. 2007). 4U 1820−30 also exhibited a super-burst during *RXTE* observations (Strohmayer & Brown 2002), most probably resulting from a burning of a large mass of carbon. Theoretical modeling of the bursts from 4U 1820−30 agrees well with the observations for a pure He or a hydrogen-poor companion depending on the assumed value for the time-averaged accretion rate (Cumming 2003).

In this study, we analyze time-resolved X-ray spectra of the photospheric radius expansion bursts observed from the low-mass X-ray binary 4U 1820−30. Using the distance measurements to the globular cluster NGC 6624 and the observed spectral parameters, we determine the mass of the neutron star in this binary to be $M = 1.58 \pm 0.06\,M_{\odot}$ and its radius to be $R = 9.11 \pm 0.40$ km. Finally, we show that only the smaller value of the two existing distance measurements to the globular cluster is consistent with the spectroscopic data.

2. THE DISTANCE TO NGC 6624

NGC 6624 is a metal-rich globular cluster with an iron abundance of $[\mathrm{Fe/H}] = -0.63 \pm 0.1$ that is determined from high resolution infrared spectroscopy with the WFPC2 camera on the *Hubble Space Telescope* (Heasley et al. 2000; see also Piotto et al. 2002). This makes its metallicity very close to that of the globular cluster 47 Tuc. Currently, there are two separate distance measurements to this globular cluster, performed in the optical and near-IR bands.

The first of these measurements is by Kuulkers et al. (2003), based on the observations of Heasley et al. (2000) in the optical band. Using a foreground reddening of $E_{B-V} = 0.32 \pm 0.03$, the apparent magnitude of the horizontal branch $V_{\mathrm{HB}} = 16.10 \pm 0.05$, and the metallicity quoted above, they derive a distance of 7.6 ± 0.4 kpc. In this measurement, the absolute calibration of distance is carried out according to the relation given by Harris (1996).

The second and more recent measurement is reported as part of a systematic exploration of the near-IR properties of 24 globular clusters in the galactic bulge (Valenti et al. 2007). In their catalog[1], Valenti et al. (2007) present the photometric properties, the reddening, and the distances of these clusters. For NGC 6624, they find a reddening and a distance of $E_{B-V} = 0.28$ and $D = 8.4$ kpc, respectively. These results are based on a comparison of color–magnitude diagrams (CMDs) and the luminosity functions of a cluster with that of a reference cluster. For metal-rich clusters such as NGC 6624, 47 Tuc is taken as the reference cluster. The combined error on the distance modulus is taken to be ~ 0.15 mag, which includes the error on the comparison of the CMDs and the luminosity functions with those of 47 Tuc as well as the uncertainty of the distance to the reference cluster (E. Valenti 2008, private communication). This translates to a distance error of 0.6 kpc.

[1] http://www.bo.astro.it/~GC/ir_archive

Table 1
Column Density in Various Elements Measured by Juett et al. (2004, 2006) with *Chandra* HETG Observations Toward 4U 1820−30

Element	N_X	Equivalent $N_{\rm H}$
O	$(1.3 \pm 0.1) \times 10^{18}$	$(2.7 \pm 0.2) \times 10^{21}$
Ne	$(3.3 \pm 0.6) \times 10^{17}$	$(3.8 \pm 0.7) \times 10^{21}$
Fe	$(5.1 \pm 0.9) \times 10^{16}$	$(1.9 \pm 0.4) \times 10^{21}$

The two distance measurements are consistent within their formal uncertainties. In our calculations, we give equal probability to each and allow for the distances $d = 6.8 - 9.6$ kpc, spanning a range that is 2σ from the central values of each measurement.

3. SPECTRAL ANALYSIS OF X-RAY BURSTS

4U 1820−30 was observed with *RXTE* for a total of 1230 ks until 2007 June (Galloway et al. 2008). However, the majority of the observations were performed when the persistent flux of the source was above the critical limit, beyond which thermonuclear bursts are not triggered. Consequently, only five thermonuclear X-ray bursts were detected in the data set (Galloway et al. 2008; see also Zdziarski et al. 2007). The ratio of the persistent flux to the peak burst flux during these five bursts is in the 5% to 7% range.

We extracted time resolved 2.5−25.0 keV X-ray spectra using the ftool *seextrct* for the science event mode data and *saextrct* tool for the science array mode data from all the *RXTE*/PCA layers. Science mode observations provide high count-rate data with a nominal time resolution of 125μs in 64 spectral channels over the whole energy range (2–60 keV) of the Proportional Counter Array (PCA) detector. We binned the X-ray spectra in 26 spectral channels and over 0.25 s for count rates above 6000 counts s^{-1} and over 0.5 s for count rates between 6000−3000 counts s^{-1}. Some data gaps during the observations, however, necessitated the extraction of X-ray spectra with smaller exposure times in a few cases. We also extracted a spectrum for the 16 s intervals prior to the bursts and used it as background. We generated separate response matrix files for each burst using the PCARSP version 11.7, HEASOFT release 6.7, and HEASARC's remote calibration database, and took into account the offset pointing of the PCA during the creation of the response matrix files. This latest version of the PCA response matrix makes the instrument calibration self-consistent over the PCA lifetime and yields a normalization of the Crab pulsar that is within 1σ of the calibration measurement of Toor & Seward (1974) for that source.

To analyze the spectra, we used the Interactive Spectral Interpretation System (ISIS), version 1.4.9–55 (Houck & Denicola 2000). We fit each spectra with a blackbody function using the *bbodyrad* model (as defined in XSPEC; Arnaud 1996) and with *tbabs* (Wilms et al. 2000) to model interstellar extinction. In each fit, we included a systematic error of 0.5% as suggested by the *RXTE* calibration team[2].

When fitting the burst spectra, we made use of the detailed interstellar extinction measurements towards 4U 1820−30 performed by Juett et al. (2004) and Juett et al. (2006) using *Chandra* high energy transmission grating observations. The column density values for O, Ne, and Fe that were measured in these studies by modeling the K and L shell absorption edges are shown in Table 1. Note that the 2σ error bars given in Juett et al. (2004, 2006) have been converted to 1σ error bars in Table 1 for consistency with the rest of the paper. We also converted the column density of each element to an equivalent hydrogen column density using interstellar medium (ISM) abundances (Wilms et al. 2000), as shown in the last column. Given the statistical agreement between these measurements, we calculated their weighted average and found $N_{\rm H} = (2.5 \pm 0.3) \times 10^{21}$ cm^{-2}, where the error denotes the 1σ uncertainty. When fitting burst spectra, we fixed the hydrogen column density at this value in the *tbabs* model. We note that converting the reddening, $E(B-V) = 0.32 \pm 0.03$, measured by Heasley et al. (2000) using the conversion $N_{\rm H} = (6.86 \pm 0.27) \times 10^{21} \times E(B-V)$ (Güver & Özel 2009) yields an equivalent hydrogen column density of $(2.20 \pm 0.22) \times 10^{21}$ cm^{-2}, which is in agreement with the value given above.

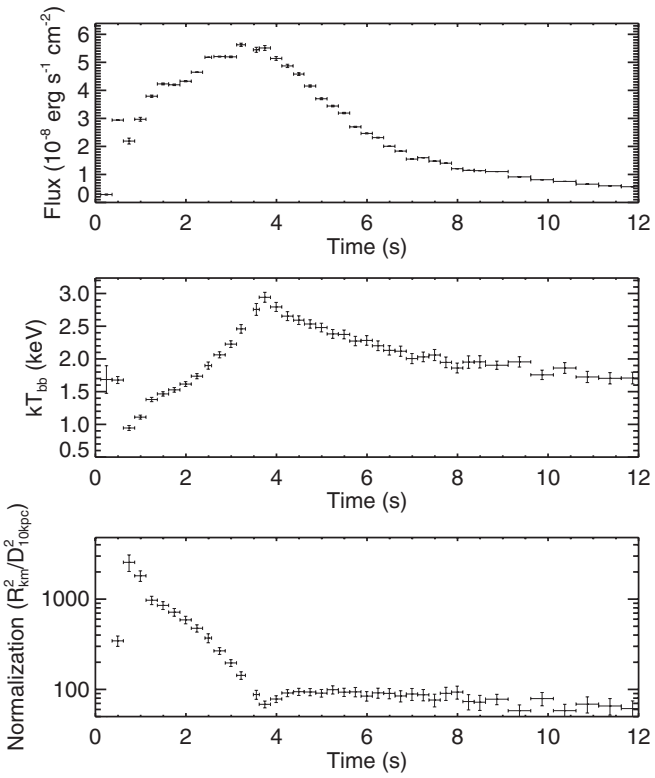

Figure 1. Spectral evolution during the first 12 s of an example burst of 4U 1820−30 (Obs id : 90027-01-03-05).

We found that all five bursts observed from 4U 1820−30 in the *RXTE* archive were photospheric radius expansion bursts, following the characteristic evolution of temperature, flux, and normalization associated with such bursts. In Figure 1, we present the evolution of the spectral parameters during an example photospheric radius expansion burst from this source. We used Equation (3) of Galloway et al. (2008) to calculate the bolometric fluxes. All the errors given show the 1σ confidence levels of our fits.

Following Özel et al. (2009) and Güver et al. (2010), we determined the touchdown flux as the bolometric flux measured when the normalization of the blackbody obtains its lowest value and the temperature reaches its highest value. In Table 2 and Figure 2, we show the results of the touchdown flux measurements. Even though the errors in the blackbody normalization and the spectral temperature are correlated, the touchdown flux involves a product of these quantities. This is shown in Figure 2 as dashed curves corresponding to constant touchdown

[2] http://www.universe.nasa.gov/xrays/programs/rxte/pca/doc/rmf/pcarmf-11.7/

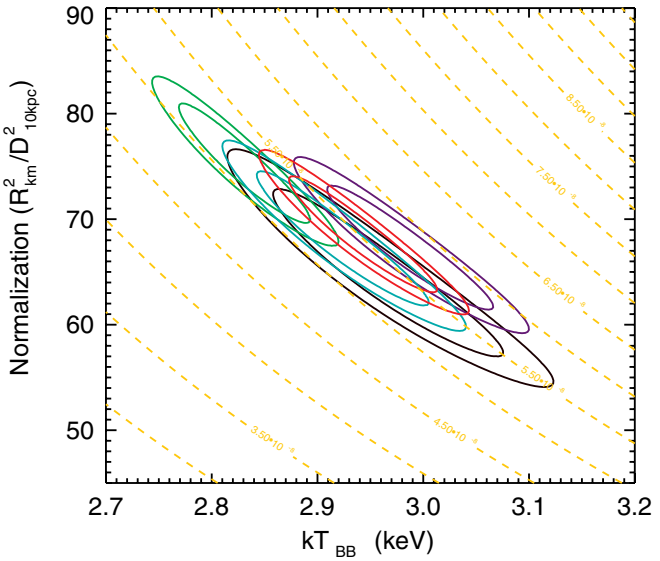

Figure 2. 1 and 2σ confidence contours of the normalization and blackbody temperature obtained from fitting the five X-ray spectra extracted from the touchdown moments of 5 PRE bursts observed from 4U 1820−30. The dashed lines show contours of constant bolometric flux.

(A color version of this figure is available in the online journal.)

Table 2
Touchdown Flux and Normalization Measurements for the PRE Bursts Observed from 4U 1820−30

Obs. ID	MJD	Touchdown Flux (10^{-8} erg cm^{-2} s^{-1})	Normalization $(R_{km}/D_{10\,kpc})^2$
20075-01-05-00	50570.73110	5.36 ± 0.27	...
40017-01-24-00	52794.73813	5.75 ± 0.20	88.86 ± 3.96
70030-03-04-01	52802.07557	5.19 ± 0.15	96.68 ± 3.39
70030-03-05-01	52805.89566	5.34 ± 0.20	...
90027-01-03-05	53277.43856	5.51 ± 0.17	90.40 ± 2.69

flux levels, and can be determined with much higher precision than either quantity. All five PRE bursts show touchdown fluxes that are statistically consistent with each other. We obtained the distribution of touchdown fluxes from the probability distributions over normalization and temperature and determined the combined 1 and 2σ confidence levels. We found an average touchdown flux of $(5.39 \pm 0.12) \times 10^{-8}$ erg cm^{-2} s^{-1}.

The second spectral quantity we measure is the normalization of the blackbody attained during the cooling tails of the thermonuclear bursts. The normalization, as defined in the XSPEC model *bbodyrad*, is related to the apparent blackbody radius and the distance through $A = (R_{app}/D_{10\,kpc})^2$, where R is the apparent radius of the neutron star and D is the distance in units of 10 kpc. In Figure 3, we show the distribution of the χ^2_ν values that we obtained during the cooling tails of each burst and compare it to the expected distribution for 26 degrees of freedom. All of the spectral fits follow the expected distribution and are statistically acceptable. In order to find the average normalization for each burst, we took the measurements for the time intervals 4.25–8 s after each burst started, when the apparent radius remained constant while the flux remained high enough for a reliable determination of spectral parameters. Constant blackbody normalizations were clearly observed in three bursts. In Figure 4, we show the histogram of all the normalization values obtained from the blackbody fits and overplot the Gaussian distribution with a standard deviation equal to the average statistical error of the individual measurements. It is evident from

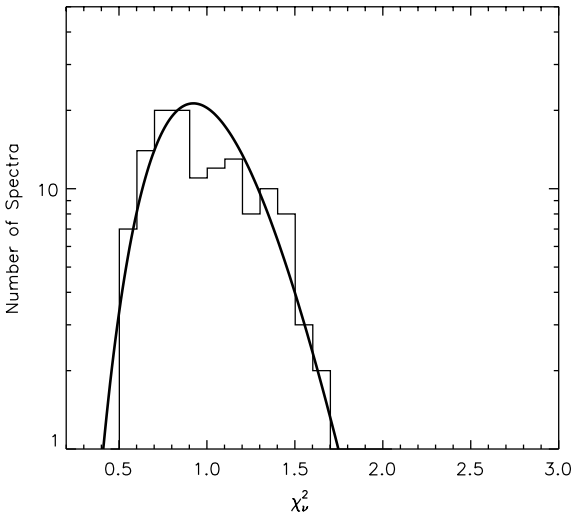

Figure 3. Histogram of χ^2_ν values obtained from spectral fitting of X-ray spectra during the cooling tail of all X-ray bursts observed from 4U 1820−30. The thick line shows the expected χ^2_ν distribution for 26 degrees of freedom.

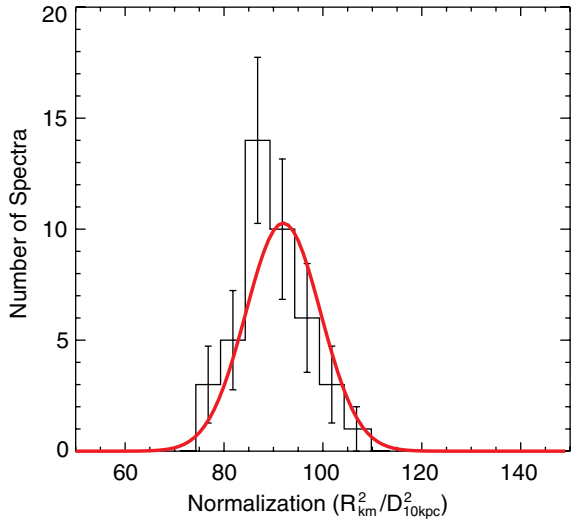

Figure 4. Histogram of all normalization measurements from cooling tails of three X-ray bursts observed from 4U 1820−30. The red line shows the Gaussian distribution with a sigma of 11.5, which is similar to the average of the statistical errors of individual measurements.

(A color version of this figure is available in the online journal.)

Figure 4 that the normalization values follow the expected normal distribution and are in very good agreement with a single apparent radius. Additionally, in Figure 5, we show the evolution of the bolometric flux and the blackbody temperature during the cooling tails of the three bursts, which also shows that the evolution of the bolometric flux and the blackbody temperature values follow the expected $F \propto T^4$ relation.

The statistical errors in the spectral parameters increase towards lower fluxes and this may affect our search for any possible systematic variations in the normalization. In principle, this effect can be alleviated by increasing the integration time of each spectrum. However, given the rapid spectral evolution during X-ray bursts, using longer exposure times for each X-ray spectrum typically leads to statistically worse fits because the extracted spectra are broadened by the variation in the temperature and the source flux. This may also affect the inferred best fit values. With that caveat, we extracted X-ray spectra for longer exposure times (0.5 and 1 s) and analyzed the re-binned spectra with the same method outlined above. We

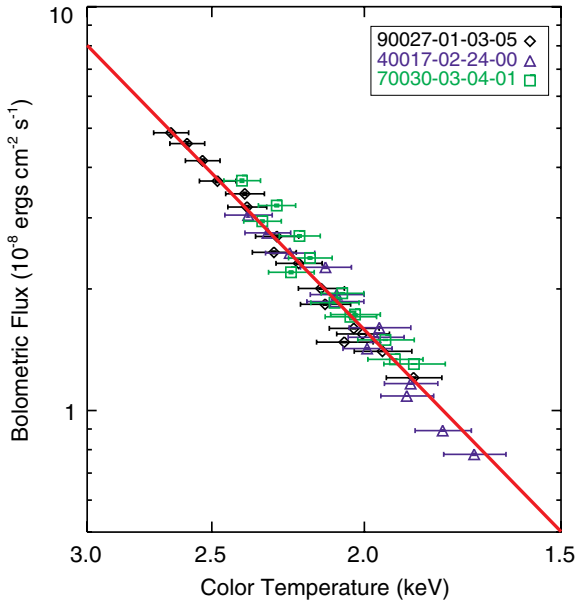

Figure 5. Evolution of bolometric flux and blackbody temperature during the cooling tails of three thermonuclear X-ray bursts observed from 4U 1820−30. Bursts follow the $L \propto T^4$ relation, which is indicated by the solid line.

(A color version of this figure is available in the online journal.)

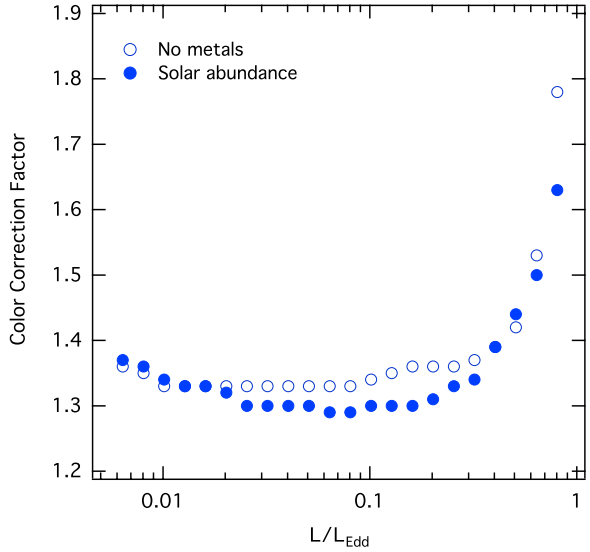

Figure 6. Evolution of the color correction factor with luminosity, in units of the Eddington luminosity, for atmosphere models with zero metallicity (open circles) and with solar metal abundances (filled circles). These data points correspond to two sequences of models from the calculations of Madej et al. (2004; zero metallicity) and Majczyna et al. (2005; solar abundances) that span the widest range of luminosities.

(A color version of this figure is available in the online journal.)

then fit the dependence of normalization on temperature with a linear relation. Even in this case, the data are consistent within 2σ with no evolution of the normalization with decreasing temperature. The best-fit linear model corresponds to a drop in the normalization from 95.9 $(\mathrm{km}/10\,\mathrm{kpc})^2$ when the temperature was 2.7 keV to 88.7 $(\mathrm{km}/10\ \mathrm{kpc})^2$ when the temperature dropped to 1.9 keV. This corresponds to a change of 8% in the normalization. In our analysis, we allow for a 30% systematic error in the conversion from the normalization to the apparent surface area of the neutron star by considering color correction factors in the range 1.3–1.4 (the apparent area scales as f_c^4, see Equation (2)). A possible 8% variation in the normalization is within this systematic uncertainty.

The color correction factor is indeed expected to increase at low flux levels, and lead to a reduction in the apparent surface area. For reasonable values of metal abundances in the photosphere, such small variations in the blackbody normalization at low fluxes are apparent in the calculations of Madej et al. (2004) and Majczyna et al. (2005) (see Figure 6).

The remaining two bursts had, however, more significant and continuous fluctuations in the apparent radii, while one of the two also showed an overall declining trend. Both the fluctuations and the overall trend cannot be explained by a simple spectral evolution but indicate uneven burning or cooling in the burst layer. Therefore, these two bursts cannot be used to measure the radius of the neutron star. We, thus, excluded them from radius measurements. The results are shown in Table 2. Formally fitting the three measurements with a constant, we obtained a blackbody normalization of $91.98 \pm 1.86\ (\mathrm{km}/10\ \mathrm{kpc})^2$.

4. MEASUREMENT OF THE MASS AND THE RADIUS OF THE NEUTRON STAR

The observed spectral quantities depend on the stellar mass and radius according to the equations (see, e.g., Özel et al. 2009).

$$F_{\mathrm{TD}} = \frac{GMc}{\kappa_{es} D^2}\left(1 - \frac{2GM}{Rc^2}\right)^{1/2} \tag{1}$$

$$A = \frac{R^2}{D^2 f_c^4}\left(1 - \frac{2GM}{Rc^2}\right)^{-1}, \tag{2}$$

where G is the gravitational constant, c is the speed of light, κ_{es} is the opacity to electron scattering, and f_c is the color correction factor.

We assign independent probability distribution functions to the distance $\mathrm{P}(D)dD$, the touchdown flux $P(F_{\mathrm{TD}})dF_{\mathrm{TD}}$, normalization $P(A)dA$, the hydrogen mass fraction $P(X)dX$, and the color correction factor $P(f_c)df_c$ that are based on the measurements, theoretical models, or known priors. We then calculate the total probability density over the neutron star mass M and radius R by integrating the equation

$$\begin{aligned} &P(D, X, f_c, M, R)dDdXdf_cdMdR \\ &\quad = \frac{1}{2}P(D)P(X)P(f_c)P[F_{\mathrm{TD}}(M, R, D, X)] \\ &\qquad \times P[A(M, R, D, f_c)]J\left(\frac{F_{\mathrm{TD}}, A}{M, R}\right)dDdXdf_cdMdR, \end{aligned} \tag{3}$$

over the distance, the hydrogen mass fraction, and the color correction factor. Here, $J(F_{\mathrm{TD}}, A/M, R)$ is the Jacobian of the transformation from the variables (F_{TD}, A) to (M, R).

The measurements of the touchdown flux and the normalization were presented in Section 3. Because the different measurements in both cases agree within their formal statistical errors, we assume a Gaussian probability distribution for each of these measurements. For the touchdown flux, we take

$$P(F_{\mathrm{TD}})dF_{\mathrm{TD}} = \frac{1}{\sqrt{2\pi\sigma_F^2}}\exp\left[-\frac{(F_{\mathrm{TD}} - F_0)^2}{2\sigma_F^2}\right] \tag{4}$$

with $F_0 = 5.39 \times 10^{-8}$ erg cm^{-2} s^{-1} and $\sigma_F = 0.12 \times 10^{-8}$ erg cm^{-2} s^{-1}. Similarly, for the normalization, we assume

a Gaussian probability distribution, i,e.,

$$P(A)dA = \frac{1}{\sqrt{2\pi\sigma_A^2}} \exp\left[-\frac{(A-A_0)^2}{2\sigma_A^2}\right] \quad (5)$$

with $A_0 = 91.98$ (km/10 kpc)^2 and $\sigma_A = 1.86$ (km/10 kpc)^2.

Previous studies have yielded two different distance measurements for the globular cluster NGC 6624, 7.6 ± 0.4 kpc from optical (Kuulkers et al. 2003) and 8.4 ± 0.6 kpc from near-IR observations (Valenti et al. 2007). In the absence of any further constraint on the distance to the cluster, we assume a box-car probability distribution, allowing it to cover the range from 6.8 to 9.6 kpc, i,e.,

$$P(D)dD = \begin{cases} \frac{1}{\Delta D} & \text{if} |D - D_0| \leqslant \Delta D/2 \\ 0 & \text{otherwise,} \end{cases} \quad (6)$$

based on the errors provided by each measurement.

The color correction factor that is obtained from modeling the hot atmospheres of accreting, bursting neutron stars was discussed in detail in Güver et al. (2010). The calculations show that when the thermal flux is in the range between $\approx 1\%$–50% sub-Eddington, the color correction factor shows little dependence on surface gravity or temperature and asymptotes to a well-determined value (e.g., Madej et al. 2004; also see Figure 11 in Güver et al. 2010). Because the color correction is applied to spectra during the cooling tails of the bursts when the flux is indeed significantly sub-Eddington, we adopt a color correction factor of $f_c = 1.35 \pm 0.05$ that is appropriate for this regime and accounts for the range of computed values. We, thus, take a box-car probability distribution covering the range 1.3–1.4 so that

$$P(f_c)df_c = \begin{cases} \frac{1}{\Delta f_c} & \text{if} |f_c - f_{c0}| \leqslant \Delta f_c/2 \\ 0 & \text{otherwise,} \end{cases} \quad (7)$$

where $f_{c0} = 1.35$ and $\Delta f_c = 0.1$ as stated above.

We use the electron scattering opacity $\kappa_{\rm es} = 0.20(1 + X)$ cm^2 g^{-1}, which depends on the hydrogen mass fraction X. There is compelling evidence that the accreted material in 4U 1820−30 is either pure He or hydrogen poor (Nelson et al. 1986). We, therefore, take the hydrogen mass fraction X to be 0 in this case. Note that allowing the hydrogen mass fraction to vary between $X = 0.0 - 0.3$ does not affect the final mass-radius contours for this particular source because there are no consistent (M, R) solutions for the larger X values.

The probability distribution over the neutron star mass and radius can then be obtained by inserting each probability distributions into Equation (3) and integrating over the distance and the hydrogen mass fraction. Figure 7 shows the 1 and 2σ confidence contours for the mass and the radius of the neutron star in 4U 1820−30.

5. DISCUSSION

We used time-resolved X-ray spectroscopy of the thermonuclear bursts exhibited by the ultra-compact X-ray binary 4U 1820−30, in conjunction with the distance measurement to its host globular cluster NGC 6624, to obtain a measurement of the mass and radius of its neutron star. We present the resulting 1 and 2σ confidence contours of the two-dimensional probability density $P(M, R)$ in Figure 7. The peak of the distribution and the projected 1σ errors correspond to a mass of $M = 1.58 \pm 0.06\, M_\odot$ and a radius of $R = 9.11 \pm 0.4$ km.

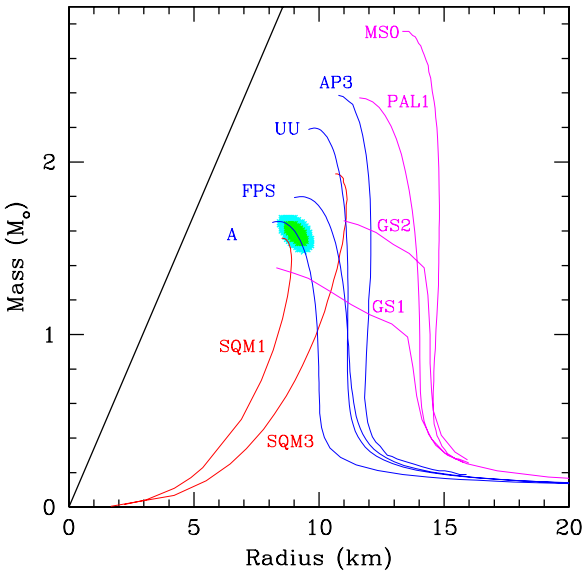

Figure 7. 1 and 2σ contours for the mass and radius of the neutron star in 4U 1820−30 are shown together with the predicted mass–radius relations for a number of equation of states of neutron star matter. The representative mass-radius relations for a select number of equations of state include multi-nucleonic ones (A, FPS, UU, AP3), equations of state with condensates (GS1-2), strange stars (SQM1, SQM3), and meson-exchange models (MS0). The black line indicates the black hole event horizon. The descriptions of the various equations of state and the corresponding labels can be found in Lattimer & Prakash (2001) and Cook et al. (1994).

(A color version of this figure is available in the online journal.)

Given the relatively large uncertainty in the source distance, the small uncertainties in the measured mass and radius call for an elucidation. The probability density over mass and radius is found by Bayesian analysis, which assigns a probability to each (M, R) pair based on the likelihood that the measured touchdown flux and the apparent emitting area can be simultaneously reproduced by that mass and radius pair, for a given distance. In the case of 4U 1820−30, the likelihood drops rapidly towards larger source distances, making the touchdown flux and the apparent emitting area practically inconsistent with each other, for any (M,R) pair. Thus, the smaller distance to the globular cluster is a posteriori favored by the spectroscopic data.

A mass measurement for the neutron star in 4U 1820−30 was reported by Zhang et al. (1998) (see also Kaaret et al. 1999 and Bloser et al. 2000) based on the measurement of the frequencies of kHz QPOs from that source. In these studies, an apparent flattening of the dependence of the upper kHz QPO frequency on X-ray count rate was interpreted as evidence for the accretion disk being truncated at the radius of the innermost stable circular orbit. The frequency of the kHz QPO at that instant was equal to ∼1060 Hz, which, if interpreted as a Keplerian frequency at the inner edge of the accretion disk, resulted in a mass for the neutron star of $\simeq 2.2\, M_\odot$. The interpretation of Zhang et al. (1998) has been questioned later by Méndez et al. (1999), who showed that the X-ray count rate is not a good indicator of mass accretion rate onto the neutron star. The highest observed QPO frequency from 4U 1820−30 can, therefore, only be used to place an upper bound on the mass of the neutron star of $\simeq 2.2\, M_\odot$ (Miller et al. 1998), which is consistent with our mass measurement.

More recently, Cackett et al. (2008) reported a measurement of the inner radius of the optically thick region of the accretion disk in 4U 1820−30 based on the modeling of the relativistically broadened iron line in the X-ray spectrum of the source observed with *Suzaku*. They estimated the inner radius of the disk to be $R_{\rm in}/M = 6.7^{+1.4}_{-0.7}$, where all quantities are expressed in geometric units. Our best-fit value for the compactness of the neutron star is $R/M \simeq 3.9$, which is smaller than the value reported by Cackett et al. (2008) for the accretion disk, as expected. The gravitational redshift corresponding to this stellar compactness is $z \simeq 0.43$.

The mass and radius reported here are also consistent with the broad constraints obtained on neutron star properties by observations of other low-mass X-ray binaries in quiescence (Rutledge et al. 2002; Heinke et al. 2006; Webb & Barret 2007). Comparing with the two measurements of neutron star masses and radii we reported earlier using the present method (Özel et al. 2009; Güver et al. 2010), we note that the neutron star in 4U 1820−30 has the smallest mass of the three (although the three span a relatively narrow range), while its radius is comparable to those of the other two neutron stars. The small differences in the masses may result from the unique accretion histories of the sources and are anticipated. All three, on the other hand, are systematically more massive than double radio pulsars, likely due to their long-lived accretion phases.

We have shown in earlier work that a wide range of ultradense matter equations of state can be well represented by the pressures specified at three fiducial densities above the nuclear saturation density. The pressures at these three densities, in turn, can be measured if a minimum of three well-constrained neutron star masses and radii are available (Özel & Psaltis 2009). The mass and radius of 4U 1820−30 represents the third such measurement and, in principle, allows for an inversion from masses and radii to the equation of state parameters. The resulting implications for the ultradense matter equation of state will be explored in a forthcoming paper.

We are grateful to Dimitrios Psaltis for various discussions. We thank the anonymous referee for very useful suggestions. We thank Elena Valenti, Sergio Ortolani, and Bill Harris for useful discussions on the distance measurements to globular clusters. F.Ö. thanks the Institute for Theory and Computation at Harvard University, where this work was completed, for their hospitality. This work was supported in part by NSF grant AST 07-08640.

REFERENCES

Anderson, S. F., Margon, B., Deutsch, E. W., Downes, R. A., & Allen, R. G. 1997, ApJ, 482, L69
Arnaud, K. A. 1996, in ASP Conf. Ser. 101, Astronomical Data Analysis Software and Systems V, ed. G. H. Jacoby & J. Barnes (San Francisco, CA: ASP), 17
Arons, J., & King, I. R. 1993, ApJ, 413, L121
Bloser, P. F., Grindlay, J. E., Kaaret, P., Zhang, W., Smale, A. P., & Barret, D. 2000, ApJ, 542, 1000
Cackett, E. M., et al. 2008, ApJ, 674, 415
Cook, G. B., Shapiro, S. L., & Teukolsky, S. A. 1994, ApJ, 424, 823
Cumming, A. 2003, ApJ, 595, 1077
Galloway, D. K., Muno, M. P., Hartman, J. M., Psaltis, D., & Chakrabarty, D. 2008, ApJS, 179, 360
Grindlay, J., Gursky, H., Schnopper, H., Parsignault, D. R., Heise, J., Brinkman, A. C., & Schrijver, J. 1976, ApJ, 205, L127
Güver, T., & Özel, F. 2009, MNRAS, 400, 2050
Güver, T., Özel, F., Cabrera-Lavers, A., & Wroblewski, P. 2010, ApJ, 712, 964
Harris, W. E. 1996, AJ, 112, 1487
Heasley, J. N., Janes, K. A., Zinn, R., Demarque, P., Da Costa, G. S., & Christian, C. A. 2000, AJ, 120, 879
Heinke, C. O., Rybicki, G. B., Narayan, R., & Grindlay, J. E. 2006, ApJ, 644, 1090
Houck, J. C., & Denicola, L. A. 2000, in ASP Conf. Ser. 216, Astronomical Data Analysis Software and Systems IX, ed. N. Manset, C. Veillet, & D. Crabtree (San Francisco, CA: ASP), 591
Juett, A. M., Schulz, N. S., & Chakrabarty, D. 2004, ApJ, 612, 308
Juett, A. M., Schulz, N. S., Chakrabarty, D., & Gorczyca, T. W. 2006, ApJ, 648, 1066
Kaaret, P., Piraino, S., Bloser, P. F., Ford, E. C., Grindlay, J. E., Santangelo, A., Smale, A. P., & Zhang, W. 1999, ApJ, 520, L37
Kuulkers, E., den Hartog, P. R., in't Zand, J. J. M., Verbunt, F. W. M., Harris, W. E., & Cocchi, M. 2003, A&A, 399, 663
Lattimer, J. M., & Prakash, M. 2001, ApJ, 550, 426
Madej, J., Joss, P. C., & Różańska, A. 2004, ApJ, 602, 904
Majczyna, A., Madej, J., Joss, P. C., & Różańska, A. 2005, A&A, 430, 643
Méndez, M., van der Klis, M., Ford, E. C., Wijnands, R., & van Paradijs, J. 1999, ApJ, 511, L49
Miller, M. C., Lamb, F. K., & Psaltis, D. 1998, ApJ, 508, 791
Nelson, L. A., Rappaport, S. A., & Joss, P. C. 1986, ApJ, 304, 231
Özel, F., Güver, T., & Psaltis, D. 2009, ApJ, 693, 1775
Özel, F., & Psaltis, D. 2009, Phys. Rev. D, 80, 103003
Piotto, G., et al. 2002, A&A, 391, 945
Rutledge, R. E., Bildsten, L., Brown, E. F., Pavlov, G. G., Zavlin, V. E., & Ushomirsky, G. 2002, ApJ, 580, 413
Stella, L., White, N. E., & Priedhorsky, W. 1987, ApJ, 315, L49
Strohmayer, T. E., & Brown, E. F. 2002, ApJ, 566, 1045
Toor, A., & Seward, F. D. 1974, AJ, 79, 995
Valenti, E., Ferraro, F. R., & Origlia, L. 2007, AJ, 133, 1287
Verbunt, F. 1987, ApJ, 312, 23
Webb, N. A., & Barret, D. 2007, ApJ, 671, 727
Wilms, J., Allen, A., & McCray, R. 2000, ApJ, 542, 914
Zdziarski, A. A., Gierliski, M., Wen, L., & Kostrzewa, Z. 2007, MNRAS, 377, 1017
Zhang, W., Smale, A. P., Strohmayer, T. E., & Swank, J. H. 1998, ApJ, 500, L171